ARTICLE
Journal of Cellular Biochemistry 112:1532–1543 (2011)

Journal of Cellular Biochemistry

A Peptide Corresponding to the C-terminal Region of Pleiotrophin Inhibits Angiogenesis In Vivo and In Vitro

Constantinos Mikelis,[1] Margarita Lamprou,[1] Marina Koutsioumpa,[1] Alexandros G. Koutsioubas,[2] Zinovia Spyranti,[3] Aikaterini A. Zompra,[4] Nikolaos Spiliopoulos,[3] Alexandros A. Vradis,[2] Panagiotis Katsoris,[5] Georgios A. Spyroulias,[3] Paul Cordopatis,[4] Jose Courty,[6] and Evangelia Papadimitriou[1*]

[1]*Laboratory of Molecular Pharmacology, Department of Pharmacy, University of Patras, Patras 26504, Greece*

[2]*Department of Physics, University of Patras, Patras 26504, Greece*

[3]*Department of Pharmacy, University of Patras, Patras 26504, Greece*

[4]*Laboratory of Pharmacognocy and Chemistry of Natural Products, Department of Pharmacy, University of Patras, Patras 26504, Greece*

[5]*Department of Biology, University of Patras, Patras 26504, Greece*

[6]*Laboratoire CRRET, Université Paris Est, EAC 7149 CNRS, Avenue du Général de Gaulle, Créteil Cedex 94010, France*

ABSTRACT

Pleiotrophin (PTN) is a heparin-binding growth factor that plays a significant role in tumor growth and angiogenesis. We have previously shown that in order for PTN to induce migration of endothelial cells, binding to both $\alpha_v\beta_3$ integrin and its receptor protein tyrosine phosphatase beta/zeta (RPTPβ/ζ) is required. In the present study we show that a synthetic peptide corresponding to the last 25 amino acids of the C-terminal region of PTN ($PTN_{112-136}$) inhibited angiogenesis in the in vivo chicken embryo chorioallantoic membrane (CAM) assay and PTN-induced migration and tube formation of human endothelial cells in vitro. $PTN_{112-136}$ inhibited binding of PTN to $\alpha_v\beta_3$ integrin, and as shown by surface plasmon resonance (SPR) measurements, specifically interacted with the specificity loop of the extracellular domain of β_3. Moreover, it abolished PTN-induced FAK Y397 phosphorylation, similarly to the effect of a neutralizing $\alpha_v\beta_3$-selective antibody. $PTN_{112-136}$ did not affect binding of PTN to RPTPβ/ζ in endothelial cells and induced β_3 Y773 phosphorylation and ERK1/2 activation to a similar extent with PTN. This effect was inhibited by down-regulation of RPTPβ/ζ by siRNA or by c-src inhibition, suggesting that $PTN_{112-136}$ may interact with RPTPβ/ζ. NMR spectroscopy studies showed that $PTN_{112-136}$ was characterized by conformational flexibility and absence of any element of secondary structure at room temperature, although the biologically active peptide segment 123–132 may adopt a defined structure at lower temperature. Collectively, our data suggest that although $PTN_{112-136}$ induces some of the signaling pathways triggered by PTN, it inhibits PTN-induced angiogenic activities through inhibition of PTN binding to $\alpha_v\beta_3$ integrin. J. Cell. Biochem. 112: 1532–1543, 2011.

KEY WORDS: INTEGRIN; RECEPTOR PROTEIN TYROSINE PHOSPHATASE; ENDOTHELIAL CELLS; MIGRATION; HEPARIN AFFIN REGULATORY PEPTIDE; NMR; SOLUTION STRUCTURE

Pleiotrophin (PTN) is an 18 kDa highly conserved heparin-binding growth factor with many biological activities. PTN is expressed in many types of cells and cell lines, among which are tumor and endothelial cells and is considered a tumor-promoting and angiogenic growth factor [Mikelis et al., 2007; Papadimitriou et al., 2009]. PTN induces human endothelial cell migration through binding to both receptor protein tyrosine phosphatase beta/zeta (RPTPβ/ζ) [Polykratis et al., 2005] and $\alpha_v\beta_3$ integrin, with the latter

Supporting information may be found in the online version of this article.

Grant sponsor: E.U. European Social Fund (75%) and the Greek Ministry of Development-GSRT (25%); Grant number: PENED 036Δ560.

Constantinos Mikelis's present address is Oral and Pharyngeal Cancer Branch, National Institute of Dental and Craniofacial Research, National Institutes of Health, 30 Convent Drive, Building 30, Room 203, Bethesda, MD 20892-4340, USA.

Alexandros G. Koutsioubas's present address is Laboratoire Léon Brillouin, CEA-CNRS, CEA Saclay, Gif-sur-Yvette F-91191, France.

*Correspondence to: Evangelia Papadimitriou, Laboratory of Molecular Pharmacology, Department of Pharmacy, University of Patras, Patras 26504, Greece. E-mail: epapad@upatras.gr

Received 23 August 2010; Accepted 3 February 2011 • DOI 10.1002/jcb.23066 • © 2011 Wiley-Liss, Inc.

Published online 22 February 2011 in Wiley Online Library (wileyonlinelibrary.com).

being the determinant of a stimulatory or inhibitory effect of PTN on cell migration [Mikelis et al., 2009]. Although the regions of both RPTPβ/ζ [Maeda et al., 1996; Bao et al., 2005] and $\alpha_v\beta_3$ [Mikelis et al., 2009] that are involved in their interaction with PTN have been at least partially identified, the region(s) of PTN that interact with its receptors have not been determined.

Different regions of PTN may exert distinct, or even opposite, effects on tumor growth and angiogenesis [Zhang et al., 1999; Polykratis et al., 2004], although the data existing so far do not lead to clear conclusions. The last 25 aminoacids of the C-terminal region of PTN are not involved in the neurite outgrowth activity of PTN [Bernard-Pierrot et al., 2001], but seem to be involved in its mitogenic and tumor promoting activities. No signal transduction was detected in PTNΔ111–136 mutant over-expressing cells, suggesting absence of PTN binding to its receptor(s) when it lacks its C-terminal region [Bernard-Pierrot et al., 2001]. Furthermore, the PTNΔ111–136 mutant protein was shown to act as a dominant negative mutant of PTN's mitogenic, angiogenic, transforming and tumor formation activities in MDA-MB231 [Bernard-Pierrot et al., 2002; Duces et al., 2008] and U87MG [Dos Santos et al., 2010] cells. Finally, a synthetic peptide corresponding to aminoacids 112–136 of wild type PTN ($PTN_{112-136}$) displayed in vitro inhibition of wild type PTN activities in NIH-3T3 and MDA-MB 231 cells and reduced PTN binding to the extracellular domain of its receptor anaplastic lymphoma kinase (ALK) [Bernard-Pierrot et al., 2002] or RPTPβ/ζ [Bermek et al., 2007].

In the present work we studied the effect of $PTN_{112-136}$ on angiogenesis in vivo and in vitro. Furthermore, the conformational properties and the solution structure of the $PTN_{112-136}$ peptide were determined through NMR spectroscopy, in an effort to relate structure with its biological activities.

MATERIALS AND METHODS

ANTIBODIES AND REAGENTS

Cell culture reagents were from BiochromKG (Seromed, Germany). Human recombinant PTN was from Peprotech Inc. (Rocky Hill, NJ). Antibodies against PTN were from Santa Cruz Biotechnology Inc. (Santa Cruz, CA) and Abnova (Heidelberg, Germany), monoclonal antibody against $\alpha_v\beta_3$ (LM609) was from Chemicon (Temecula, CA), antibody against phospho-β_3(Y773) was from Abcam (Cambridge, MA), antibodies against RPTPβ/ζ and β_3 integrin were from Santa Cruz Biotechnology Inc., antibody against phospho-ERK1/2 on Thr^{202}–Tyr^{204} was from Cell Signaling (Danvers, MA), and antibody against ERK1/2 was from Upstate Biotechnology (Lake Placid, NY). FACE FAK ELISA kit to determine FAK Y397 phosphorylation was purchased from Active Motif Europe (Rixensart, Belgium). Protein A and G agarose beads were purchased from Merck (Whitehouse Station, NJ). B3 and B3 scrambled peptides were from Cambridge Peptides Ltd. (Birmingham, UK). RNA oligonucleotide primers for RPTPβ/ζ [Polykratis et al., 2005] were obtained from VBCBiotech Services (Vienna, Austria) and the transfection reagent JetSI-ENDO was from Polyplus Transfection, Illkirch, France. All secondary horseradish peroxidase-conjugated antibodies were purchased from Sigma (St. Louis, MO) and all other reagents were purchased from Sigma or Applichem (Darmstadt, Germany).

$PTN_{112-136}$ AND PTN_{1-5} PEPTIDE SYNTHESIS

$PTN_{112-136}$ (LTKPKPQAESKKKKKEGKKQEKMLD) and PTN_{1-5} (GKKEK) peptides were synthesized using 2-chlorotrityl-chloride resin [Barlos et al., 1991] as solid support bearing a Rink-Bernatowitz linker to provide the peptide amide [Bernatowicz et al., 1989]. Chain extension was carried out using standard Fmoc (9-fluorenylmethyloxycarbonyl) protocols [Fields and Noble, 1990; Zompra et al., 2007]. In summary, the Fmoc group was removed with 20% piperidine in *N*,*N*-dimethylformamide (DMF). Activation of each amino acid was performed in situ using diisopropylcarbodiimide/1-hydroxybenzotriazol (DIC/HOBt) in DMF. Treatment of the peptidyl resin with trifluoroacetic acid/dichloromethane/1,2-ethanedithiol/anisole/water (80:10:5:3:2, v/v) for 4 h afforded the desired product. Peptides were precipitated upon evaporation in vacuo and addition of ether. The crude peptides were purified by gel filtration chromatography on Sephadex G-15 using 15% acetic acid as eluent. Final purification was achieved by preparative HPLC (Mod.10 ÄKTA, Amersham Biosciences) on reversed-phase support C-18 with a linear gradient from 5 to 50% acetonitrile (0.1% TFA) for 40 min at a flow rate 2.0 ml/min. Analytical HPLC equipped with a C-18 Phase Sep column S3 ODS2 produced single peak with at least 98% of the total peptide peak integral. Electro-spray MS was in agreement with the expected results.

CHORIOALLANTOIC MEMBRANE (CAM) ANGIOGENESIS ASSAY

The in vivo chicken embryo CAM angiogenesis assay was used, as previously described [Papadimitriou et al., 2001]. Leghorn fertilized eggs (Pindos, Ioannina, Greece) were incubated for 4 days at 37°C, when a window was opened on the egg shell, exposing the CAM. The window was covered with tape and the eggs were returned to the incubator. Different amounts of the peptides were diluted in a final volume of 20 μl H_2O and applied at the ninth day of embryo development on an area of 1 cm^2 of the CAM, restricted by a plastic ring. Forty eight hours after treatment and subsequent incubation at 37°C, CAMs were fixed in situ, excised from the eggs, placed on slides and left to air-dry. Pictures were taken through a stereoscope equipped with a digital camera and the total length of the vessels was measured. Briefly, vessel length was measured by adjusting all vessels of a picture of defined dimensions, to one pixel thickness. The vessel area was then expressed as the percentage of pixels occupied by the 1-pixel-thick vessels in the picture and was quantified using ImagePC image analysis software (Scion Corporation, Frederick, MD). Assays were carried out at least three times and each experiment contained 10–20 eggs per data point.

CELL CULTURE

Human umbilical vein endothelial cells (HUVEC) were isolated from human umbilical cords and grown as monolayers in medium M199 that was supplemented with 15% fetal bovine serum, 150 mg/ml endothelial cell growth supplement, 5 U/ml heparin sodium, 100 U/ml penicillin–streptomycin, 50 mg/ml gentamycin, and 2.5 mg/ml amphotericin B [Polykratis et al., 2005; Mikelis et al., 2009]. When cells reached 80–90% confluence, they were serum-starved for 16 h before performing migration, tube formation and phosphorylation assays, or lysed for immunoprecipitation assays.

MIGRATION ASSAYS

Migration assays were performed in 24-well microchemotaxis chambers (Costar) using uncoated polycarbonate membranes with 8 μm pores [Polykratis et al., 2005; Mikelis et al., 2009]. Serum starved cells were harvested and resuspended at a concentration of 10^5 cells/0.1 ml in M199 containing 0.25% bovine serum albumin (BSA). The bottom chamber was filled with 0.6 ml of M199 containing 0.25% BSA and the tested substances. The upper chamber was loaded with 10^5 cells and incubated for 4 h at 37°C. After completion of the incubation, the filters were fixed and stained with 0.33% toluidine blue solution. The cells that migrated through the filter were quantified by counting the entire area of each filter, using a grid and an Optech microscope at a 20× magnification.

MATRIGEL TUBE FORMATION ASSAY

Growth factor-reduced Matrigel™ was used to coat the wells of 96-well tissue culture plates (0.04 ml/well) and was left to polymerize for 1 h at 37°C. After polymerization, 1.5×10^4 cells suspended in 0.15 ml of M199 were added to each well. The tested agents were added in the medium and 6 h after incubation at 37°C, the medium was removed, the cells were fixed and stained with Diff Quick (Baxter Scientific). Photographs were taken through a stereoscope equipped with a digital camera and the length of the tube network was measured in the total area of the wells after having adjusted all tubes to one pixel thickness. The tube area was expressed as the percentage of pixels occupied by the 1-pixel-thick tubes and was quantified using ImagePC image analysis software [Polykratis et al., 2005].

RNA INTERFERENCE

HUVEC were grown to a confluence of 40% in medium without antibiotics. Transfection was performed in serum-containing medium for 4 h using annealed RNA for RPTPβ/ζ at the concentration of 50 nM and JetSI-ENDO as transfection reagent [Polykratis et al., 2005; Mikelis et al., 2009]. Cells were incubated for another 48 h in serum-containing medium and then, they were serum-starved before further experiments. Double-stranded negative control siRNA (Ambion Inc.) was used in all experiments.

IMMUNOPRECIPITATION AND WESTERN BLOT ASSAYS

Immunoprecipitation assays were performed as previously described [Mikelis et al., 2009]. Briefly, when cells were grown to 90% confluence in the presence or absence of $PTN_{112-136}$, the medium was aspirated, cells were washed twice with ice-cold phosphate buffered saline pH 7.4 (PBS) and lysed with PBS containing 1% Triton X-100, 0.1% SDS, 20 nM sodium orthovanadate, 1 μg/ml aprotinin, 1 mM phenylmethylsulfonyl fluoride, and 5 mM EDTA. Cells were scraped off the plate, transferred to eppendorf tubes, kept on ice for 30 min, and centrifuged at 20,000 g for 30 min at 4°C. 1–3 mg of supernatant were transferred to new eppendorf tubes and incubated with primary antibody for 16 h at 4°C under continuous agitation. Protein A- and protein G-agarose beads were added and samples were further incubated for 2 h at 4°C. Beads and bound proteins were collected by centrifugation and washed twice with ice-cold PBS. The pellet was resuspended in 50 μl SDS loading buffer, heated to 95–100°C for 5 min and centrifuged. In the case of signaling molecules, cells were serum-starved and then incubated with the tested agents for 15 min, after which they were directly lysed in SDS loading buffer. In all cases, proteins were analyzed by SDS–PAGE and transferred to Immobilon P membranes. Blocking was performed by incubating the membranes with Tris-buffered saline pH 7.4, with 0.05% Tween (TBS-T), containing 3% BSA. Membranes were further incubated with primary antibodies for 16 h at 4°C under continuous agitation, washed three times with TBS-T, and incubated with secondary antibodies for 1 h at room temperature. Membranes were finally washed and detection of immunoreactive bands was performed using the ECL detection kit (Pierce), according to the manufacturer's instructions. Blots for pY773β_3 and pERK1/2 were stripped and subjected to subsequent Western blotting for total β_3 and ERK1/2, respectively. The protein levels that corresponded to the immunoreactive bands were quantified using the ImagePC image analysis software.

ELISA FOR MEASUREMENT OF FAK Y397 PHOSPHORYLATION

Phosphorylation of FAK at Y397 was measured using the Fast Activated Cell-based ELISA kit by Active Motif, following the manufacturer's instructions. Briefly, when cells reached 80% confluency in 96-well plates, they were serum-starved for 24 h and then incubated with the tested agents for 15 min. Cells were fixed using 4% formaldehyde in PBS, washed and further incubated with primary and secondary antibodies as suggested by the manufacturer. Absorbance was measured using an ELISA reader at 450 nm with a reference wavelength of 655 nm.

SPR ASSAY

The SPR measurements were performed using a homemade apparatus previously described [Koutsioubas et al., 2006]. Briefly, surface plasmons are excited (under the Kretschmann configuration) by a p-polarized laser beam ($\lambda = 632.8$ nm) on thin ~50 nm gold films that are prepared by vacuum evaporation on the face of an optically flat SF10 high refractive index ($n = 1.723$) equilateral prism. Buffers and solutions are brought into contact with the gold surface using a custom made PTFE cell. SPR reflectance curves are fitted [Koutsioubas et al., 2007] assuming that the adsorbed molecular layers are homogeneous and that the refractive index of the peptides is equal to 1.45 [Schmid et al., 2006]. Stable immobilization of $PTN_{112-136}$ peptide on the gold surface was achieved by the formation of a dithiobissuccinimide proprionate (DSP) self-assembled monolayer (SAM) on the gold surface [Schmid et al., 2006]. More specifically, freshly evaporated gold films were exposed to a 0.002 M DSP prepared in dimethylsulfoxide (DMSO) for 1.5 h at room temperature. SPR measurements revealed that a DSP SAM is quickly formed on the gold surface due to disulfide linkage. After reaction, the gold surface was rinsed with DMSO and then with PBS. A 0.005 μg/μl $PTN_{112-136}$ peptide solution prepared in PBS was introduced into the cell and the amine groups of the $PTN_{112-136}$ peptide covalently replaced the NHS groups of the DSP SAM molecules [Shonam et al., 1995]. The surface was rinsed with PBS and a 0.005 μg/μl B3 or scrambled B3 peptide solution prepared in PBS was injected into the cell, in order to study the interaction between B3 or scrambled B3 peptide and the $PTN_{112-136}$ coated gold surface.

NMR SPECTROSCOPY

Data were acquired at 278 and 298 K on a Bruker Avance 700-MHz spectrometer. ^{1}H 1D NMR spectra was recorded using spectral width of 12–17 ppm with or without presaturation of the H_2O signal. ^{1}H-^{1}H 2D TOCSY [Braunschweiler and Ernst, 1983; Bax and Davis, 1985] spectra was recorded using the MLEV-17 spin lock sequence using $\tau_m = 70$ ms and ^{1}H-^{13}C HSQC [Bax and Grzesiek, 1993] spectra with 200.791 p.p.m. spectral width in F1. ^{1}H-^{1}H TPPI NOESY [Jeener et al., 1979; Marion and Wüthrich, 1983] spectra was acquired using mixing time $\tau_m = 300$ ms applying water suppression during the relaxation delay and mixing time. All homonuclear ^{1}H-^{1}H 2D spectra were acquired with 10.014 ppm spectral width, consisting of 2K data points in the F2 dimension, 16–32 transients, and 512–1024 complex increments in the F1 dimension. Raw data were multiplied in both dimensions by a pure cosine-squared bell window function and Fourier-transformed to obtain 2048 × 2048 real data points. A polynomial base-line correction was applied in both directions. For data processing and spectral analysis, the standard Bruker software (XWinNMR 3.5) and XEASY program [Eccles et al., 1991] (ETH, Zurich) were used.

NOE constraints. Six hundred forty NOESY cross-peaks were assigned in both dimensions for the $PTN_{112-135}$ peptide in H_2O. The number of meaningful NOE was 176, that is nine constraints per residue. Their intensities were converted into upper limit distances through CALIBA [Güntert et al., 1991]. Sequential constraints, number, and range of NOEs are illustrated in supplementary Figure S1.

Structure calculations and refinement. The NOE-derived structural information extracted from the analysis of NOESY spectrum acquired in H_2O solutions under identical experimental conditions for the $PTN_{112-136}$ peptide and was introduced to DYANA [Wüthrich et al., 1983; Güntert et al., 1997] software for structure calculation. The peptide models in Figure 7 have been generated with MOLMOL [Koradi et al., 1996]. Structural calculations have been performed on IBM RISC6000 and xw4100/xw4200 HP Linux workstations.

STATISTICAL ANALYSIS

All experiments were performed at least three independent times. The significance of variability between the results from each group and the corresponding control was determined by unpaired *t*-test. The significance of variability among the results from various groups (different concentrations or different treatments) was determined by one-way ANOVA.

RESULTS

$PTN_{112-136}$ INHIBITED ANGIOGENESIS IN VIVO

The effect of $PTN_{112-136}$ on physiological angiogenesis was studied in vivo, using the chicken embryo CAM assay. As shown in Figure 1, $PTN_{112-136}$ caused a small, but statistically significant and dose-dependent decrease of the total vessel length, reaching a maximum inhibition at the concentration of 1 μg/cm^2. A control peptide that corresponds to the first five aminoacids of the N-terminal region of PTN (PTN_{1-5}) and is also positively charged had no effect on the CAM angiogenesis. $PTN_{112-136}$ at all concentrations used in the present study was not toxic on the CAM cells, as verified on CAM paraffin sections stained with eosin-haematoxylin (data not shown).

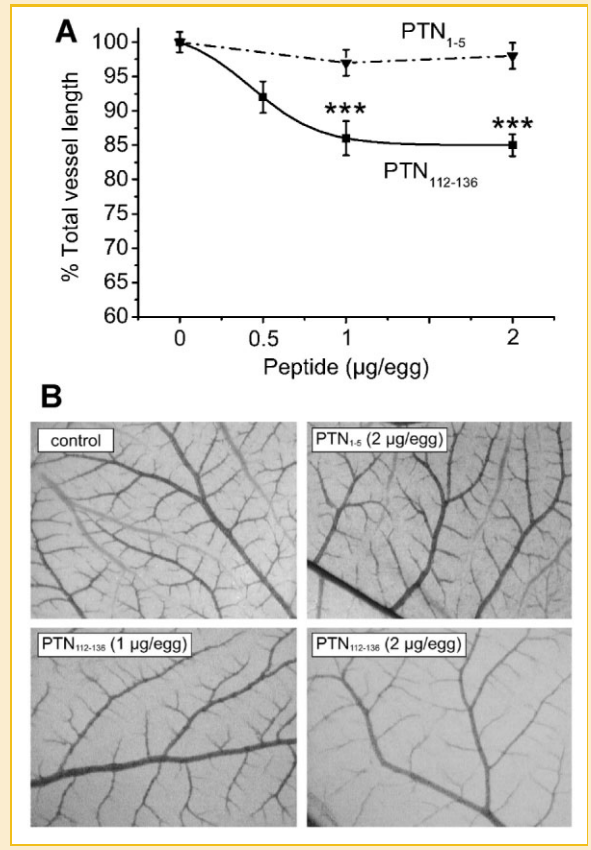

Fig. 1. Inhibition of in vivo angiogenesis by $PTN_{112-136}$. (A) Different amounts of $PTN_{112-136}$ or PTN_{1-5} in the same final volume of 20 μl were applied on an area of 1 cm^2 restricted by a plastic ring at CAMs from day 9, as described in Materials and Methods. After 48 h of incubation at 37°C, the CAMs were fixed, excised from eggs, photographed, and the total length of the vessel network was measured using image analysis software. Results are expressed as mean ± s.e. of the percent length of CAM vessels compared with the untreated tissue. Asterisks denote a statistically significant difference from untreated tissue. $^{**}P < 0.01$, $^{***}P < 0.001$. (B) Representative pictures showing the vessel network of the chicken embryo CAM in the presence or absence of PTN_{1-5} or $PTN_{112-136}$.

$PTN_{112-136}$ INHIBITED IN VITRO HUMAN ENDOTHELIAL CELL MIGRATION AND TUBE FORMATION ON MATRIGEL

In order to identify the effect of $PTN_{112-136}$ on in vitro angiogenesis, we studied its effect on angiogenic functions of HUVEC such as migration and tube formation on matrigel. $PTN_{112-136}$ caused a small but statistically significant inhibition of HUVEC migration, while it completely inhibited PTN-induced migration (Fig. 2A). Similarly, $PTN_{112-136}$ inhibited both basal (non-stimulated) and PTN-induced tube formation on matrigel (Fig. 2B). In all in vitro assays, the PTN concentration used (100 ng/ml) was the one that we have previously found to cause the maximum stimulation of cell migration and tube formation on matrigel [Polykratis et al., 2005]. This concentration corresponds to 6.5 nM, which is within the amounts measured in vivo [Li et al., 2007].

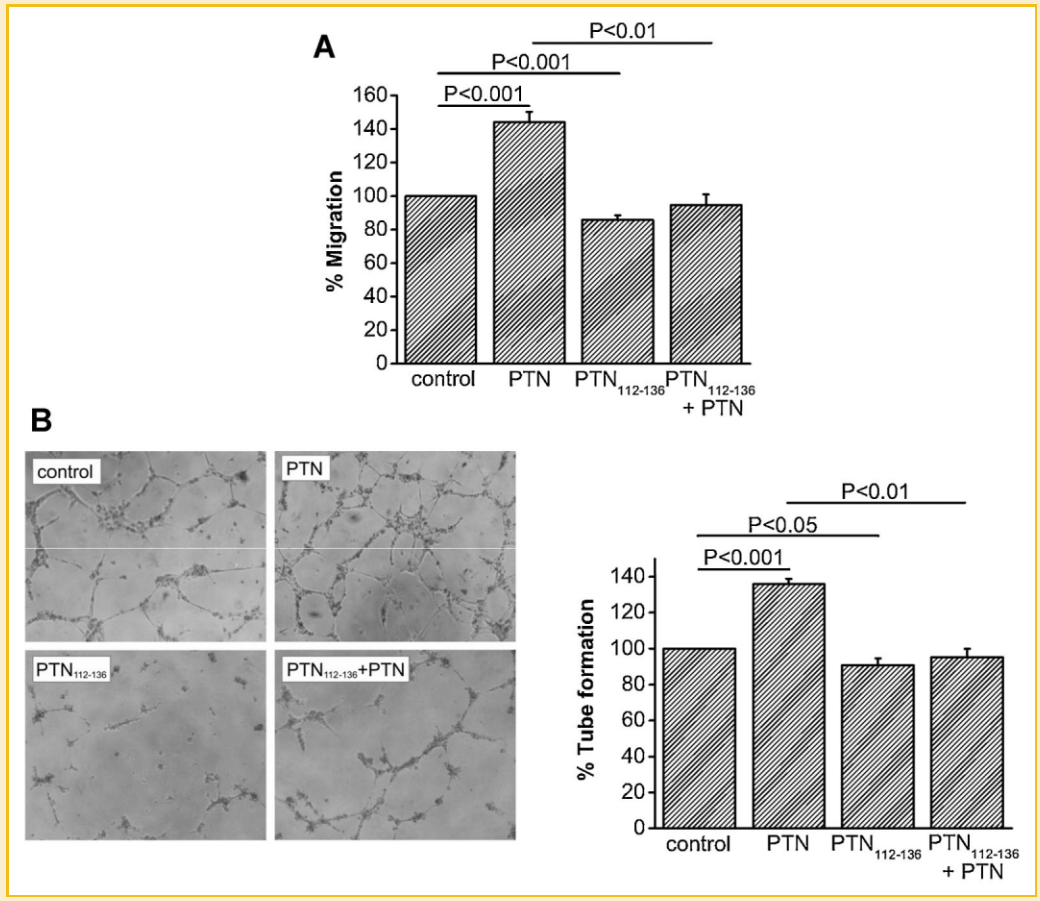

Fig. 2. Inhibition of in vitro angiogenesis by $PTN_{112-136}$. Effect of PTN (100 ng/ml), $PTN_{112-136}$ (100 ng/ml) or their combination (each at 100 ng/ml) on HUVEC migration (A) and tube formation on matrigel (B). Results are expressed as percent of values obtained without any stimulation (control). Data are the mean ± s.e. of at least three independent experiments. Pictures shown in (B) are representative of the tube network formed in the presence or absence of the tested agents.

$PTN_{112-136}$ AFFECTED THE INTERACTION OF PTN WITH $\alpha\nu\beta_3$ INTEGRIN

Since both RPTPβ/ζ and $\alpha_\nu\beta_3$ integrin are required for PTN-induced HUVEC migration [Polykratis et al., 2005; Mikelis et al., 2009], we studied whether $PTN_{112-136}$ affects interaction of PTN with $\alpha_\nu\beta_3$, RPTPβ/ζ, or both. Cells were grown in the presence or absence of $PTN_{112-136}$ and in each case, 3 mg of total protein from cell lysates were immunoprecipitated for $\alpha_\nu\beta_3$ or RPTPβ/ζ and analyzed for the presence of PTN. $PTN_{112-136}$ inhibited interaction of PTN with $\alpha_\nu\beta_3$ (Fig. 3A) but not RPTPβ/ζ (Fig. 3B) in HUVEC.

$PTN_{112-136}$ SPECIFICALLY INTERACTED WITH THE CYSTEINE LOOP 177–184 OF THE β_3 INTEGRIN EXTRACELLULAR DOMAIN

Since PTN interacts with $\alpha_\nu\beta_3$ through the specificity loop of the β_3 integrin extracellular domain [Mikelis et al., 2009], we studied the interaction of $PTN_{112-136}$ with a synthetic peptide that corresponds to aminoacids 177–184 and mimics the cysteine loop of β_3 (B3 peptide) by using surface plasmon resonance (SPR), as described in Materials and Methods. The reaction kinetics (adsorbed mass per unit area Γ vs. time t) during immobilization of $PTN_{112-136}$ on the gold surface are illustrated in Figure 4A. We observed that the reaction reaches equilibrium at about 1500 s. Successive rinse of the surface with phosphate buffered saline pH 7.4 (PBS) did not appreciably change the $PTN_{112-136}$ adsorbed mass per unit area. The interaction between B3 or B3 scrambled peptides (analyte) and $PTN_{112-136}$ (receptor)-coated gold surface was estimated after injection into the cell of a 0.005 μg/μl B3 or B3 scrambled peptide solution prepared in PBS. Typical analyte–receptor binding kinetics are presented in Figure 4B. $PTN_{112-136}$ and B3 peptide formed a relatively high affinity complex. The affinity of B3 peptide for $PTN_{112-136}$ was much higher than the affinity of the B3 scrambled peptide. By assuming that analyte–receptor reaction is governed by first-order kinetics [Stepanek et al., 2006], we calculated the association rate constant K for both cases. We found $2.9 \times 10^4\,M^{-1}\,s^{-1}$ for the $PTN_{112-136}$–B3 peptide interaction and $2.4 \times 10^2\,M^{-1}\,s^{-1}$ for the $PTN_{112-136}$–B3 scrambled peptide interaction. It is interesting to note that at equilibrium, the B3 peptide presented almost the same adsorbed mass per unit area as the $PTN_{112-136}$ immobilized peptide. Since both B3 and scrambled B3 peptides have the same molecular weight, this observation suggests that the vast majority of receptor sites were bound to analyte and that non-specific binding is not at play.

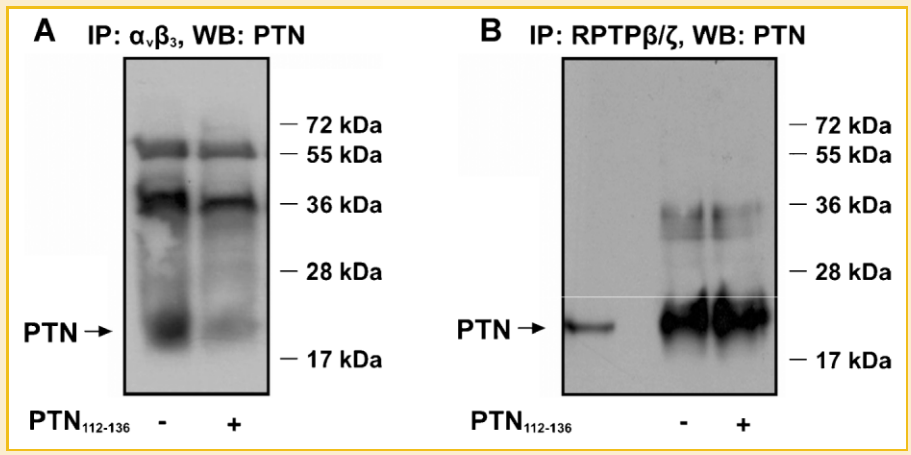

Fig. 3. $PTN_{112-136}$ inhibited interaction of PTN with $\alpha_v\beta_3$ but not RPTPβ/ζ. Three mg of total lysate protein derived from three to four 100 mm Petri dishes of untreated or treated with 100 ng/ml $PTN_{112-136}$ HUVEC were immunoprecipitated for $\alpha_v\beta_3$ integrin (A) and RPTPβ/ζ (B) and the immunoprecipitates were analyzed by Western blot for the presence of PTN. Arrows indicate the full length monomeric PTN.

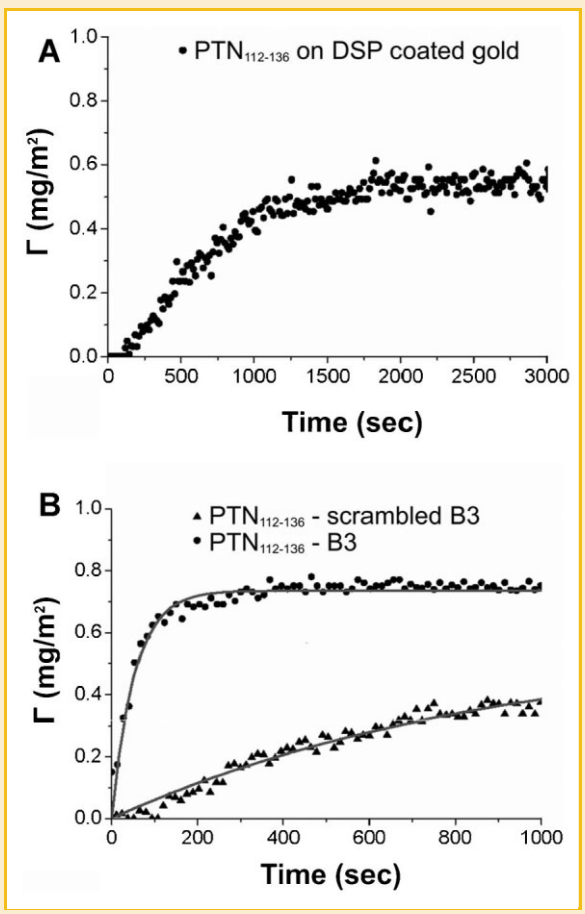

Fig. 4. Specific interaction between $PTN_{112-136}$ and B3 peptides. (A) Adsorption kinetics during $PTN_{112-136}$ covalent linkage on the DSP modified gold surface. (B) Representative (B3/B3 scrambled peptide) – (immobilized $PTN_{112-136}$) binding kinetics. The continuous curves represent first-order kinetics that fit to the experimental data.

$PTN_{112-136}$ INHIBITED PTN-INDUCED Y397 FAK PHOSPHORYLATION THROUGH INTERACTION WITH $\alpha_V\beta_3$

We have previously shown that PTN induces tyrosine phosphorylation of FAK [Polykratis et al., 2005], although phosphorylation of different tyrosine residues of FAK by PTN has not been determined. Based on the assumption that integrin-dependent Y397 auto-phosphorylation of FAK is the first step of its activation [Mitra and Schlaepfer, 2006], we studied whether PTN affects Y397 phosphorylation of FAK through $\alpha_v\beta_3$, as well as the effect of $PTN_{112-136}$. As shown in Figure 5, PTN at the concentration of 100 ng/ml that causes the maximal effect on HUVEC migration [Polykratis et al., 2005], induced Y397 FAK auto-phosphorylation, an effect completely abolished by the $\alpha_v\beta_3$ neutralizing antibody LM609 or by $PTN_{112-136}$.

$PTN_{112-136}$ INDUCED Y773 PHOSPHORYLATION OF β_3 SUBUNIT AND ACTIVATION OF ERK1/2 PROBABLY VIA RPTPβ/ζ AND c-SRC KINASE

We have previously shown that PTN induces phosphorylation of β_3 integrin on Y773 and activation of ERK1/2 through its receptor RPTPβ/ζ [Polykratis et al., 2005; Mikelis et al., 2009]. Since $PTN_{112-136}$ inhibits PTN-induced endothelial cell migration, we studied whether it also inhibits these signaling pathways that are stimulated by PTN. To our surprise, $PTN_{112-136}$ induced Y773 phosphorylation of β_3 integrin to a similar extent with PTN, an effect abolished by down-regulation of RPTPβ/ζ by siRNA or by the selective inhibitor of the downstream c-src PP1 (Fig. 6A). Similarly, $PTN_{112-136}$ induced ERK1/2 activation to a similar extent with PTN, an effect also abolished by down-regulation of RPTPβ/ζ by siRNA or by PP1 (Fig. 6B).

NMR STUDIES OF $PTN_{112-136}$

Given the binding affinity of $PTN_{112-136}$ to the cysteine loop of the β_3 integrin and the inhibition of biological activities, we tried to clarify the conformational properties of the PTN peptide that may be related to this effect. NMR data acquired at room temperature are

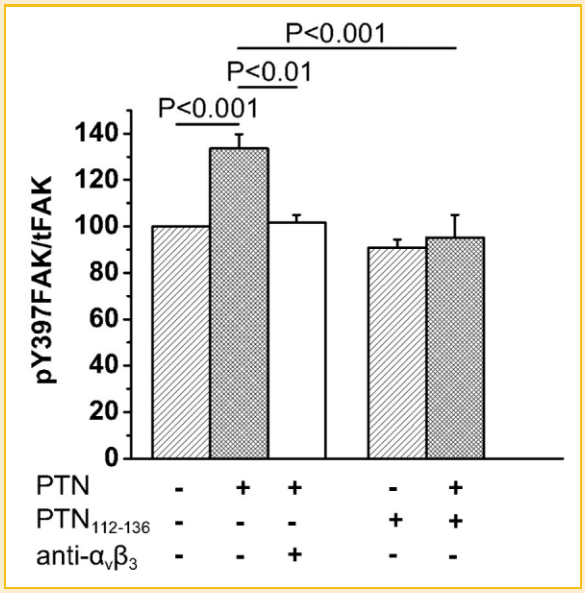

Fig. 5. $PTN_{112-136}$ inhibited PTN-induced Y397 FAK phosphorylation. HUVEC were stimulated with the tested agents for 15 min, fixed and incubated with antibodies against phospho Y397 (pY397FAK) and total (tFAK) FAK. The ratio pY397FAK/tFAK was calculated in each well. Results are mean ± s.e. of the percentage change of the relative amounts of the phosphorylated Y397 FAK in treated vs. untreated cells. PTN, cells treated with 100 ng/ml PTN; $PTN_{112-136}$, cells treated with 100 ng/ml $PTN_{112-136}$; anti-$\alpha_v\beta_3$, cells treated with 10 ng/ml LM609.

indicative for a rather flexible polypeptide skeleton. Moreover, the NOESY spectrum exhibits only a few proton–proton correlations, involving mainly backbone nuclei. Alternatively, experiments were performed at a lower temperature (278 K) in order to reduce the peptide skeleton flexibility.

Proton assignment. TOCSY maps were first analyzed to assign the individual spin patterns of amino acids through scalar connectivities (Fig. 7A). Sequential and medium-range connectivities were identified from NOESY maps acquired with $\tau_m = 300$ ms. Chemical shifts for carbon nuclei were obtained from ^{13}C-HSQC spectrum. Chemical shifts for $PTN_{112-136}$ are reported in Table I. HN-HN sequential connectivities are detected between almost all residues of the peptide sequence. H_α-HN and H_β-HN sequential connectivities are also detected in several peptide fragments (Fig. S1). Six hundred forty cross peaks were assigned in both dimensions of the NOESY spectrum for $PTN_{112-136}$ peptide, with the number of unique cross peaks reaching up to 322. The absence of the long-range NOEs is possibly due to the high flexibility of $PTN_{112-136}$ peptide in solution, as well as to the signal overlapping, because of the existence of a high number of neighboring lysines in the peptide sequence (totally 10 Lysine residues and five consecutive; Lys^{122}–Lys^{126} segment). Indeed, no long-range NOEs ($\geq$i,i + 5) could be identified in the spectra.

Structure calculations and conformational analysis. The average target function for the DYANA family of 20 calculated models (Fig. 7B–D) was found to be $0.22 \pm 2.52 \times 10^{-2}$ Å^2 for $PTN_{112-136}$ models. No consistent violations existed at the final DYANA run and no constraint violation was found larger than 0.30 Å. The final ensemble exhibits pairwise rmsd values, calculated for residues Lys^{116}–Lys^{133}, 3.85 ± 0.81 Å (BB) and 5.60 ± 0.96 Å (HA) for the 20 structures. The corresponding rmsd values for the $PTN_{123-132}$ peptide ensemble are 1.70 ± 0.70 Å (BB) and 3.70 ± 1.13 Å (HA) for the 20 models.

3D solution structures. The NMR data for $PTN_{112-136}$ suggest a conformation with no well-defined secondary structure elements for this peptide, due to the absence of any long-range and the limited number of medium-range (i,i + 3) NOEs (Fig. 7B). However, a backbone bend is formed by residues Glu^{127}–Gln^{131}, indicating the formation of a segment with local folded structure in the conformational ensemble (Fig. 7C). As far as the nature of the peptide bond for both prolines is concerned, analysis of the proline ^{13}C resonances observed for $PTN_{112-136}$, demonstrate in both cases, Pro^{115} and Pro^{117}, the existence of a dominant *trans* conformation. C_β of Pro^{115} is found to be at 33.172 ppm, while C_γ is found at 29.632 ppm. The difference in ppm is 3.54, indicating that the dominant conformation of the Lys^{114}–Pro^{115} peptide bond of the model ensemble is *trans* and that *cis–trans* isomerization is not detectable in NMR time scale. The corresponding $\Delta_{\beta\gamma}$ value for Pro^{117} is found to be 4.021, suggesting a *trans* conformation for the peptide bond between residues Lys^{116}–Pro^{117}.

DISCUSSION

In the present study we show that a synthetic peptide that corresponds to the last 25 amino acid residues of the C-terminal region of PTN inhibits PTN-induced angiogenic activity. The small but statistically significant effect of $PTN_{112-136}$ on non-stimulated endothelial cell migration and tube formation on matrigel is probably due to inhibition of the effect of the low endogenous PTN levels produced by non-stimulated serum-starved human endothelial cells [Poimenidi et al., 2009]. Similarly, its inhibitory effect on physiological angiogenesis of the chicken embryo CAM may be due to inhibition of the effect of endogenous PTN produced by CAM cells. Avian PTN is highly homologous to the corresponding human protein [Papadimitriou et al., 2009] and we found no sequence differences between human $PTN_{112-136}$ and the corresponding avian peptide. The small effect of $PTN_{112-136}$ on CAM angiogenesis could be explained by the fact that the exact amount of the peptide that can reach the responsive CAM cells is not known and is expected to be much lower than that applied onto the tissue. Moreover, CAM consists of many different types of cells besides endothelial cells, which could contribute in various ways to the final net effect of the peptide. At present, we cannot say whether the effect of $PTN_{112-136}$ is only because it directly acts on CAM endothelial cells or through action on other types of cells, e.g. monocytes. It has been suggested that one of the mechanisms through which PTN affects angiogenesis in vivo is through transdifferentiation of monocytes/macrophages into functional endothelial cells [Sharifi et al., 2006; Chen et al., 2009]. Another highly positively charged peptide PTN_{1-5} had no effect on CAM angiogenesis, suggesting that the effect of $PTN_{112-136}$ is not due to its positive charge, in line with previous data on human prostate cancer cells [Bermek et al., 2007].

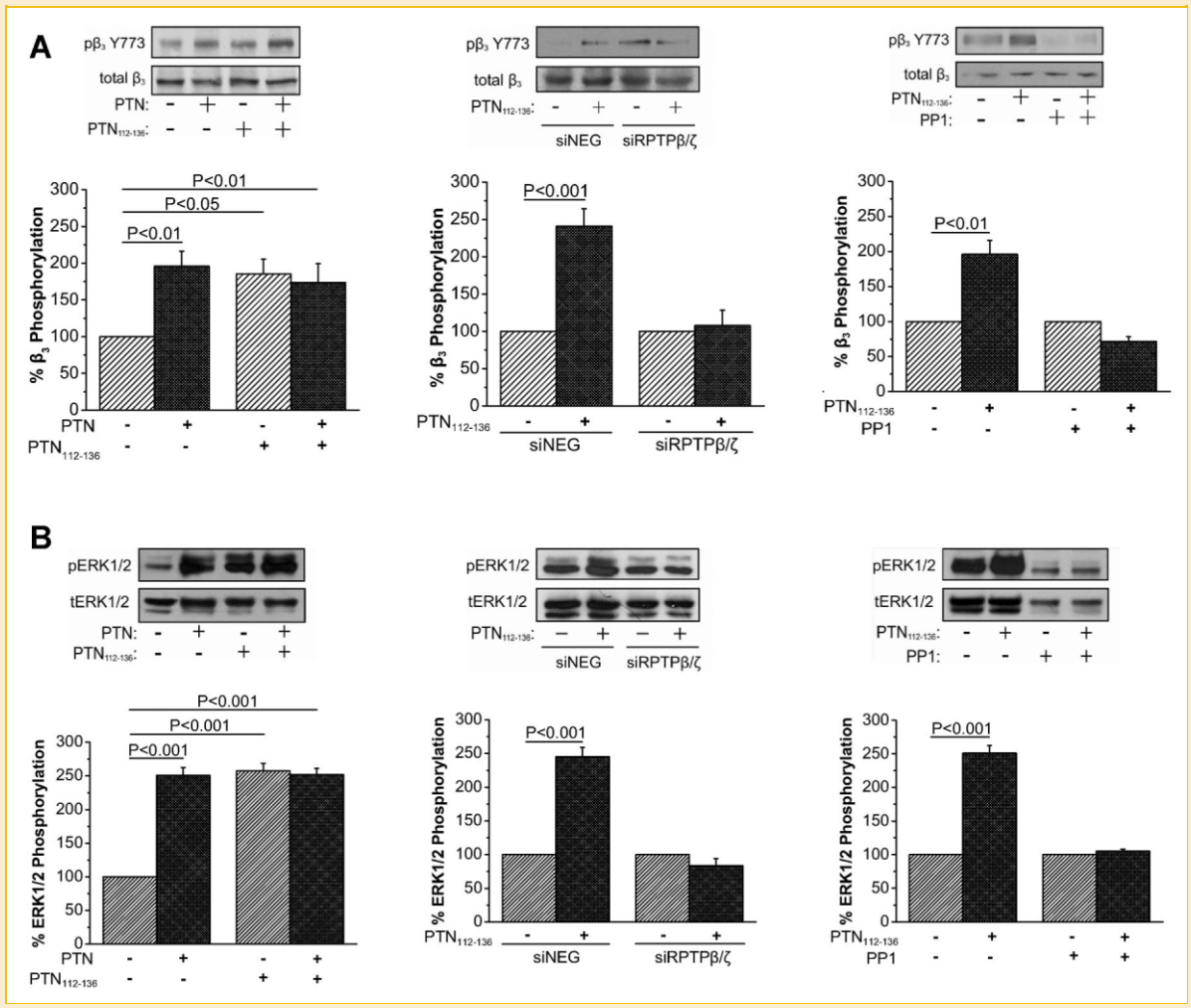

Fig. 6. $PTN_{112-136}$ induced Y773 β_3 integrin and ERK1/2 phosphorylation. HUVEC were stimulated with $PTN_{112-136}$ for 7 or 15 min for phosphorylation of β_3 integrin (A) or ERK1/2 (B) respectively. The cells were then lysed and cell lysates were analyzed by Western blot with antibodies against phospho- and total proteins. Phospho- and total protein amounts were quantified by densitometric analysis of the corresponding band in each lane, and the ratio of phospho- to the corresponding total protein was calculated in each lane. Results are mean ± s.e. of the percentage change of the relative amounts of the phosphorylated proteins in treated vs. untreated cells. siNEG, cells transfected with a negative control siRNA; siRPTPβ/ζ, cells transfected with siRNA for RPTPβ/ζ, PTN, cells treated with 100 ng/ml PTN; $PTN_{112-136}$, cells treated with 100 ng/ml $PTN_{112-136}$; PP1, cells treated with 5 μM PP1.

Although this is the first time that the effect of the C-terminal region of PTN is being studied on angiogenesis, our data are in line with previous studies showing an inhibitory effect of peptides that correspond to the C-terminal region of PTN on tumor growth [Bernard-Pierrot et al., 2002; Bermek et al., 2007]. They are also in line with data showing that PTN lacking its C-terminal region does not promote tumor growth. For example, CHO-K1 cells expressing PTNΔ111–136 mutant did not develop tumors when injected in nude mice [Bernard-Pierrot et al., 2001]. MDA-MB 231 cells that over-expressed PTNΔ111–136 together with wild type PTN formed significantly smaller tumors in nude mice compared with those expressing only wild type PTN [Bernard-Pierrot et al., 2002] and intramuscular electrotransfer of a plasmid encoding PTNΔ111–136 was shown to inhibit MDA-MB 231 tumor growth by 81% [Duces et al., 2008]. In a glioblastoma in vivo model, over-expression of PTNΔ111–136 decreased tumor cell growth in vitro and in vivo [Dos Santos et al., 2010]. Finally, matrigel injected subcutaneously in mice in the presence of both wild-type PTN and PTNΔ111–136 mutant developed reduced endothelial cell infiltration than that observed with wild type PTN alone [Bernard-Pierrot et al., 2002].

The molecules with which the C-terminal region of PTN interacts have not been identified. It has been previously suggested that PTN through its C-terminal region binds to its receptor ALK [Bernard-Pierrot et al., 2002] or RPTPβ/ζ [Bermek et al., 2007]. On the other hand, there are data showing that full length PTN acts through RPTPβ/ζ, while a form lacking the C-terminal region acts through ALK [Lu et al., 2005], favoring the notion that the C-terminal region of PTN interacts with RPTPβ/ζ or other receptor(s). In the present study, we show that the C-terminal region of PTN is responsible for binding to the Cys-loop of the β_3 subunit, playing a major role in the interaction of PTN with $\alpha_v\beta_3$ and the resulting stimulation of cell

TABLE I. ^{1}H and ^{13}C Chemical Shifts (ppm) of the Residues in $PTN_{112-136}$ at 278 K (H_2O)

Residue		HN	Hα	Hβ	Other
112	Leu	8.691	4.330		Hγ 1.428
					Cγ 39.109
113	Thr	8.716	4.434	3.757	Hγ 1.918
				66.796	Cγ 13.810
114	Lys	8.608	4.427	1.882	Hε 2.436; Hγ 1.423; Hδ 1.785
				26.500	Cε 38.905; Cγ 26.218; Cδ 20.378
115	Pro	–	4.438	2.342/2.063	Hγ 1.917
				33.172	Cγ 29.632
116	Lys	8.653	4.300	1.832/1.799	Hγ 1.508; Hδ 1.726
			51.127	29.743	Cγ 27.437
117	Pro	–	4.444	2.337/2.043	Hγ 1.906
			59.916	30.727	Cγ 26.706
118	Gln	8.674	4.302	2.057/1.950	Hγ 2.279
			51.474	33.172	Cγ 29.076
119	Ala	8.629	4.436	1.675	–
120	Glu	6.676	4.336	2.120	Hγ 2.404/2.017
				30.556	Cγ 39.218
121	Ser	8.643	4.049	3.944	–
			55.484	59.099	
122	Lys	8.432	4.302	1.846/1.778	Hγ 1.455; Hδ 1.711
				26.934	Cγ 29.206; Cδ 25.637
123	Lys	8.396	4.280	1.842/1.775	Hγ 1.496/1.439; Hδ 1.714
			52.167	29.834	Cγ 26.687; Cδ 25.059
124	Lys	8.513	4.299	1.836/1.775	Hγ 1.697; Hδ 1.476
			51.923	30.050	Cγ 30.015; Cδ 25.303
125	Lys	8.578	4.287	1.902/1.792	Hγ 1.500; Hδ 1.715
			51.622	33.166	Cγ 30.056; Cδ 24.379
126	Lys	8.420	4.329	1.838/1.776	Hγ 1.458; Hδ 1.705
			51.494		Cγ 26.231; Cδ 26.875
127	Glu	8.646	4.304	2.069/1.990	Hγ 2.323, 2.139
				27.059	Cγ 39.045
128	Gly	8.605	3.941/3.886	–	–
			49.691		
129	Lys	8.672	4.587	1.856/1.753	Hγ 1.524; Hδ 1.579
					Cγ 27.197; Cδ 27.179
130	Lys	8.558	4.323	1.837/1.793	Hγ 1.456; Hδ 1.720
					Cγ 29.646; Cδ 27.034
131	Gln	8.685	4.338	2.097	Hγ 2.329
				30.657	Cγ 39.199
132	Glu	8.032	4.374	2.685	Hγ 2.586
				39.014	Cγ 36.300
133	Lys	8.774	4.615	1.858	Hγ 1.498; Hδ 1.549
				32.715	Cγ 29.909; Cδ 29.487
134	Met	8.721	4.306	2.124	Hγ 2.443; Hε 2.340
				32.102	
135	Leu	8.498	4.416	1.690	Hδ 0.965/0.901
				29.451	Cδ 21.645
136	Asp	8.640	4.514	2.658	–
				39.014	

migration. We do not have biochemical proof of interaction of the C-terminal domain of PTN with RPTPβ/ζ in HUVEC, although we have data showing that $PTN_{112-136}$ interacts with RPTPβ/ζ in human glioma M059K cells (Sfaelou et al., unpublished observation) and $PTN_{112-136}$ induces at least part of the downstream signaling in HUVEC. Apart from the different expression of $\alpha_v\beta_3$ [Mikelis et al., 2009], we do not know what is the difference among these types of cells that may be related to the difference in the observed interaction between $PTN_{112-136}$ and RPTPβ/ζ. One possibility could be that $PTN_{112-136}$ interacts with the same region of RPTPβ/ζ that participates in the interaction with $\alpha_v\beta_3$, or that the participating region is masked by $\alpha_v\beta_3$, although further studies would be needed to address this point. Interestingly, $PTN_{112-136}$ induced Y773 phosphorylation of β_3 integrin to a similar extent with PTN, suggesting that it acts through the same pathway that involves RPTPβ/ζ and c-src [Mikelis et al., 2009]. Indeed, the stimulatory effect of $PTN_{112-136}$ on Y773 β_3 phosphorylation was abolished by selective inhibition of c-src or by down-regulation of RPTPβ/ζ, suggesting that the latter is somehow activated by $PTN_{112-136}$. We have previously shown that Y773 phosphorylation of β_3 integrin is independent of PTN binding to $\alpha_v\beta_3$, depends on RPTPβ/ζ and is not sufficient by itself to transduce the signal for PTN-induced cell migration [Mikelis et al., 2009]. In the same line, although $PTN_{112-136}$ induces Y773 β_3 phosphorylation, it does not induce HUVEC migration, further supporting the notion that signaling through RPTPβ/ζ is required but is not sufficient for PTN-induced cell migration.

Interestingly, $PTN_{112-136}$ also stimulated ERK1/2 activation to a similar extent with the whole molecule, an effect also abolished by inhibition of c-src or down-regulation of RPTPβ/ζ. Since we have previous data showing that ERK1/2 activation is required for PTN-induced HUVEC migration [Polykratis et al., 2005], it seems from the present study that it is not sufficient by itself for PTN-induced cell migration. Other signaling molecules yet to be identified are inhibited by $PTN_{112-136}$ and are responsible for its inhibitory effect on PTN-induced endothelial cell migration and angiogenesis. One

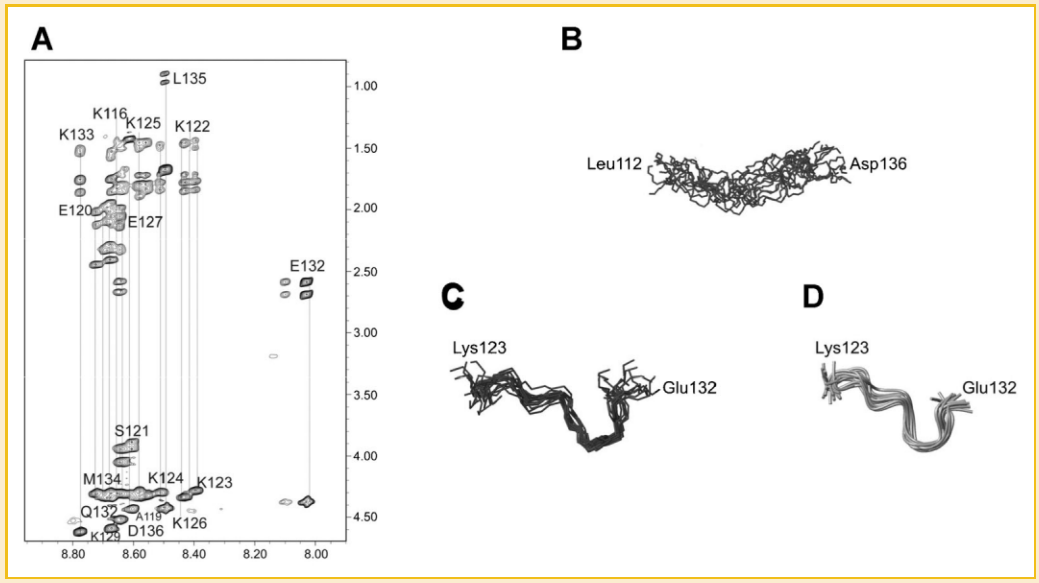

Fig. 7. (A) Characteristic TOCSY fingerprints regions of $PTN_{112-136}$ extracted from 2D ^{1}H 700-MHz NMR recorded in H_2O at 278 K. (B) The family of 20 DYANA models calculated for $PTN_{112-136}$. (C) Backbone representation of the family of 20 DYANA models calculated for $PTN_{123-132}$. (D) $PTN_{123-132}$ family ensemble illustrated as ribbon.

such molecule is FAK. PTN induces Y397 FAK phosphorylation through $\alpha_v\beta_3$, an effect completely abolished by $PTN_{112-136}$. FAK activation is required for integrin-mediated cell migration [Sieg et al., 1999] and the autophopshorylation on Y397 is prerequisite for the subsequent binding and activation from c-src [Mitra et al., 2005]. It seems that PTN binding to the cysteine loop 177–184 of $\alpha_v\beta_3$ leads to the initial activation of FAK, its interaction with the activated c-src and the induction of the migratory response, and $PTN_{112-136}$ blocks this process (Fig. 8). Further studies are in progress to elucidate the exact interplay between signaling molecules activated by $\alpha_v\beta_3$ or/and RPTPβ/ζ that results in cell migration.

In an effort to better characterize $PTN_{112-136}$ and to identify the likely minimum amino acid sequence involved in its biological activity, we elucidated the structural features of $PTN_{112-136}$ by NMR spectroscopy. The peptide proved to be highly flexible in solution at room temperature. However, the skeleton flexibility has been reduced at lower temperature and structural information was extracted. Despite the peptide's conformational flexibility even at 4°C, the $PTN_{123-132}$ segment seems to adopt a rather defined structure with the formation of a backbone turn by residues Glu^{127}–Gln^{131}, indicating a segment with a local folded structure in the conformational ensemble. As far as the side chain conformation is concerned, Glu^{127} and Gln^{131} occupy the same region in space, coming close to each other on the top of the backbone bend, while Lys^{129} and Lys^{130} hold parallel orientation with their side chains pointing outside the bend. The $PTN_{123-132}$ segment contains the basic cluster of residues at the C-terminus of PTN and has been previously shown to inhibit PTN-induced growth of human prostate cancer cells [Bermek et al., 2007]. It was then demonstrated that the specific sequence of amino acids and not the basic nature of the peptide was responsible for the effect, a notion that is also supported by our NMR data.

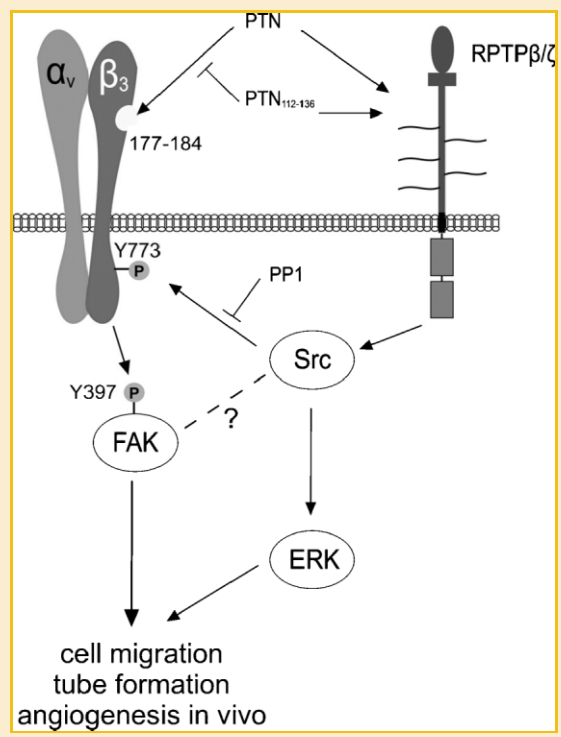

Fig. 8. PTN binds to the cysteine loop 177–184 of the β_3 subunit of $\alpha_v\beta_3$ integrin and induces phosphorylation of Y397 of FAK. Binding and subsequent activation of FAK are antagonized by $PTN_{112-136}$. Both PTN and $PTN_{112-136}$ are bound to RPTPβ/ζ and activate c-src kinase. Activation of c-src kinase induces the Y773 phosphorylation of β_3 subunit and phosphorylation of ERK. Activation of both c-src and FAK (and potential interaction) is required for the downstream in vitro and in vivo angiogenic processes and each of the pathways alone is not sufficient for this effect.

In summary, this study provides evidence that $PTN_{112-136}$ can act as a dominant negative effector of PTN-induced angiogenic in vivo and in vitro responses, through competition with PTN for binding to the extracellular domain of β_3 integrin. Moreover, it provides a tool to be used in our efforts to discriminate among the various signaling cascades that collectively participate in the angiogenic and tumorigenic activities of PTN and can lead to the development of molecules effective in controlling PTN-related pathologies.

REFERENCES

Bao X, Mikami T, Yamada S, Faissner A, Muramatsu T, Sugahara K. 2005. Heparin-binding growth factor, pleiotrophin, mediates neuritogenic activity of embryonic pig brain-derived chondroitin sulfate/dermatan sulfate hybrid chains. J Biol Chem 280:9180–9191.

Barlos K, Chatzi O, Gatos D, Stavropoulos G. 1991. 2-Chlorotrityl chloride resin. Studies on anchoring of Fmoc-amino acids and peptide cleavage. Int J Peptide Protein Res 37:513–520.

Bax A, Davis DG. 1985. MLEV-17-based two-dimensional homonuclear magnetization transfer spectroscopy. J Magn Reson 65:355–360.

Bax A, Grzesiek S. 1993. Methodological Advances in Protein NMR. Acc Chem Res 26:131–138.

Bermek O, Diamantopoulou Z, Polykratis A, Dos Santos C, Hamma-Kourbali Y, Burlina F, Delbé J, Chassaing G, Fernig DG, Katsoris P, Courty J. 2007. A basic peptide derived from the HARP C-terminus inhibits anchorage-independent growth of DU145 prostate cancer cells. Exp Cell Res 313:4041–4050.

Bernard-Pierrot I, Delbe J, Caruelle D, Barritault D, Courty J, Milhiet PE. 2001. The lysine-rich C-terminal tail of heparin affin regulatory peptide is required for mitogenic and tumour formation activities. J Biol Chem 276:12228–12234.

Bernard-Pierrot I, Delbe J, Rouet V, Vigny M, Kerros ME, Caruelle D, Raulais D, Barritault D, Courty J, Milhiet PE. 2002. Dominant negative effectors of heparin affin regulatory peptide (HARP) angiogenic and transforming activities. J Biol Chem 277:32071–32077.

Bernatowicz MS, Daniels SB, Koster H. 1989. A comparison of acid labile linkage agents for the synthesis of peptide C-terminal amides. Tetrahedron Lett 30:4645–4648.

Braunschweiler L, Ernst RR. 1983. Coherence transfer by isotropic mixing: application to proton correlation spectroscopy. J Magn Reson 53:521–528.

Chen H, Campbell RA, Chang Y, Li M, Wang CS, Li J, Sanchez E, Share M, Steinberg J, Berenson A, Shalitin D, Zeng Z, Gui D, Perez-Pinera P, Berenson RJ, Said J, Bonavida B, Deuel TF, Berenson JR. 2009. Pleiotrophin produced by multiple myeloma induces transdifferentiation of monocytes into vascular endothelial cells: a novel mechanism of tumor-induced vasculogenesis. Blood 113:1992–2002.

Dos Santos C, Karaky R, Renoir D, Hamma-Kourbali Y, Albanese P, Gobbo E, Griscelli F, Opolon P, Dalle S, Perricaudet M, Courty J, Delbé J. 2010. Antitumorigenic effects of a mutant of the heparin affin regulatory peptide (HARP) on the U87 MG glioblastoma cell line. Int J Cancer 127:1038–1051.

Duces A, Karaky R, Martel-Renoir D, Mir L, Hamma-Kourbali Y, Bieche I, Opolon P, Delbe J, Courty J, Perricaudet M, Griscelli F. 2008. 16-kDa fragment of pleiotrophin acts on endothelial and breast tumor cells and inhibits tumor development. Mol Cancer Ther 9:2817–2827.

Eccles C, Güntert P, Billeter M, Wüthrich K. 1991. Efficient analysis of protein 2D NMR spectra using the software package EASY. J Biomol NMR 1:111–130.

Fields BG, Noble LR. 1990. Solid phase peptide synthesis utilizing 9-fluorenylmethoxycarbonyl amino acids. Int J Peptide Protein Res 35:161–214.

Güntert P, Braun W, Wüthrich K. 1991. Efficient computation of three-dimensional protein structures in solution from nuclear magnetic resonance data using the program DIANA and the supporting programs CALIBA, HABAS and GLOMSA. J Mol Biol 217:517–530.

Güntert P, Mumenthaler C, Wüthrich K. 1997. Torsion angle dynamics for NMR structure calculation with the new program DYANA. J Mol Biol 273: 283–298.

Jeener J, Meier BH, Bachmann P, Ernst RR. 1979. Investigation of exchange processes by two-dimensional NMR spectroscopy. J Chem Phys 71:4546–4553.

Koradi R, Billeter M, Wüthrich K. 1996. MOLMOL: a program for display and analysis of macromolecular structures. J Mol Graph 14:51–55.

Koutsioubas AG, Spiliopoulos N, Anastassopoulos D, Vradis AA, Priftis GD. 2007. Surface Plasmon Resonance as a tool for the estimation of adsorbed layer characteristics: theoretical considerations and experiment. J Polym Sci B Polym Phys 45:2060–2070.

Koutsioubas AG, Spiliopoulos N, Anastassopoulos D, Vradis AA, Toprakcioglu C, Priftis GD. 2006. Adsorption behavior of PS-PEO diblock copolymers on silver and alumina surfaces: a surface plasmon resonance study. J Polym Sci B Polym Phys 44:1580–1591.

Li J, Wei H, Chesley A, Moon C, Krawczyk M, Volkova M, Ziman B, Margulies KB, Talan M, Crow MT, Boheler KR. 2007. The pro-angiogenic cytokine pleiotrophin potentiates cardiomyocyte apoptosis through inhibition of endogenous AKT/PKB activity. J Biol Chem 282:34984–34993.

Lu KV, Jong KA, Kim GY, Singh J, Dia EQ, Yoshimoto K, Wang MY, Cloughesy TF, Nelson SF, Mischel PS. 2005. Differential induction of glioblastoma migration and growth by two forms of pleiotrophin. J Biol Chem 280:26953–26964.

Maeda N, Nishiwaki T, Shintani T, Hamanaka H, Noda M. 1996. 6B4 proteoglycan/phosphacan, an extracellular variant of receptor-like protein tyrosine phosphatase z/RPTPb, binds pleiotrophin/heparin-binding growth associated molecule (HB-GAM). J Biol Chem 271:21446–21452.

Marion D, Wüthrich K. 1983. Application of phase sensitive two-dimensional correlated spectroscopy (COSY) for measurements of 1H-1H spin-spin coupling constants in proteins. Biochem Biophys Res Commun 113:967–974.

Mikelis C, Koutsioumpa M, Papadimitriou E. 2007. Pleiotrophin as a possible new target for angiogenesis-related diseases and cancer. Recent Patents Anticancer Drug Discov 2:175–186.

Mikelis C, Sfaelou E, Koutsioumpa M, Kieffer N, Papadimitriou E. 2009. Integrin alpha(v)beta(3) is a pleiotrophin receptor required for pleiotrophin-induced endothelial cell migration through receptor protein tyrosine phosphatase beta/zeta. FASEB J 23:1459–1469.

Mitra SK, Hanson DA, Schlaepfer DD. 2005. Focal adhesion kinase: in command and control of cell motility. Nat Rev Mol Cell Biol 6:56–68.

Mitra SK, Schlaepfer DD. 2006. Integrin-regulated FAK-src signaling in normal and cancer cells. Curr Opin Cell Biol 18:516–523.

Papadimitriou E, Mikelis C, Lampropoulou E, Koutsioumpa M, Theochari K, Tsirmoula S, Theodoropoulou C, Lamprou M, Sfaelou E, Vourtsis D, Boudouris P. 2009. Roles of pleiotrophin in tumor growth and angiogenesis. Eur Cytokine Netw 20:180–190.

Papadimitriou E, Polykratis A, Courty J, Koolwijk P, Heroult M, Katsoris P. 2001. HARP induces angiogenesis in vivo and in vitro: implication of N or C terminal peptides. Biochem Biophys Res Commun 282:306–313.

Poimenidi E, Hatziapostolou M, Papadimitriou E. 2009. Serum stimulates Pleiotrophin gene expression in an AP-1-dependent manner in human endothelial and glioblastoma cells. Anticancer Res 29:349–354.

Polykratis A, Delbe J, Courty J, Papadimitriou E, Katsoris P. 2004. Identification of heparin affin regulatory peptide domains with potential role on angiogenesis. Int J Biochem Cell Biol 36:1954–1966.

Polykratis A, Katsoris P, Courty J, Papadimitriou E. 2005. Characterization of heparin affin regulatory peptide signaling in human endothelial cells. J Biol Chem 280:22454–22461.

Schmid AH, Stanca SE, Thakur MS, Thampi KR, Suri CR. 2006. Site-directed antibody immobilization on gold substrate for surface plasmon resonance sensors. Actuators B 113:297–303.

Sharifi BG, Zeng Z, Wang L, Song L, Chen H, Qin M, Sierra-Honigmann MR, Wachsmann-Hogiu S, Shah PK. 2006. Pleiotrophin induces transdifferentiation of monocytes into functional endothelial cells. Arterioscler Thromb Vasc Biol 26:1273–1280.

Shonam B, Migram Y, Riklin A, Willner I, Tartakovsky BA. 1995. Bilirubin biosensor based on multilayer network enzyme electrode. Biosens Bioelectron 10:341–352.

Sieg DJ, Hauck CR, Schlaepfer DD. 1999. Required role of focal adhesion kinase (FAK) for integrin-stimulated cell migration. J Cell Sci 112:2677–2691.

Stepanek J, Vaisocherova H, Piliarik M. 2006. Molecular interactions in SPR sensors. In: Homola J, editor. Surface plasmon resonance based sensors. Berlin Heidelberg: Springer-Verlag. pp 69–94.

Wüthrich K, Billeter M, Brown W. 1983. Pseudo-structures for the 20 common amino acids for use in studies of protein conformations by measurements of intramolecular proton-proton distance constraints with nuclear magnetic resonance. J Mol Biol 169:949–961.

Zhang N, Zhong R, Deuel TF. 1999. Domain structure of pleiotrophin required for transformation. J Biol Chem 274:12959–12962.

Zompra AA, Magafa V, Chryssanthi DG, Lamari FN, Spyroulias GA, Maina T, Nock BA, Karamanos NK, Cordopatis P. 2007. Synthesis and biological evaluation of new GnRH analogues on pituitary and breast cancer cells. Int J Peptide Res Ther 13:143–149.